Stability of Lanthanum Strontium Manganite Catalyst with Glass Adhesive in an Electrochemical Oxidative Dehydrogenation Reactor

HONORS THESIS

Presented in Partial Fulfillment of the Requirements for the Degree Bachelors of Science with research distinction in the College of Engineering of The Ohio State University

By

Jonathan T. Davis

Program in Chemical and Biomolecular Engineering

The Ohio State University

2014

Dissertation Committee:

Professor Umit S. Ozkan, Advisor

Professor Aravind Asthagiri

Abstract

The purpose of this project is to improve the stability of a high temperature oxidative dehydrogenation (ODH) reactor. Specifically, the project investigates the interaction between the cathode catalyst and the glass material used to seal the reactor. The cathode catalyst for the experiment is 20% strontium-doped lanthanum manganite (LSM) and is commercially produced by NexTech Materials. For the experiment, LSM was cured at high temperatures with varying concentrations of glass adhesive (Aremco-Seal 617). After curing, the samples were ground into powders and characterized. X-ray diffraction was used to analyze changes in the bulk structure, while X-ray photoelectron spectroscopy (XPS) was used to analyze the composition on the surface. While LSM is shown to react with the glass seal, it was found that the material choice for wires in the reactor setup had a greater impact on electrochemical data.

Vita

May 2010 .....Grandview Heights High School

2014 (expected).....B.S. Chemical Engineering, The Ohio State University

Publications

2012.....Ce-doped strontium cobalt ferrite perovskites as cathode catalysts for solid oxide fuel cells: Effect of dopant concentration. Choi, H.; Fuller, A.; Davis, J.; Wielgus, C. Applied Catalysis B: Environmental 127:336-341.

2014 (expected).....Effect of Ce doping on the performance and stability of strontium cobalt ferrite perovskites as SOFC anode catalysts. Choi, H.; Fuller, A.; Davis, J.; Co, A.; Ozkan, U.

Fields of Study

Major Field: Chemical and Biomolecular Engineering

Table of Contents

List of Tables

List of Figures

Introduction

Propylene is an important chemical building block which is used to obtain industrial compounds such as polypropylene, acrylonitrile, propylene oxide, and many other organic intermediates [1]. Figure 1 below shows the distribution of demand for these products [2]. Typically, propylene is obtained as a byproduct from catalytically cracking naptha [3].

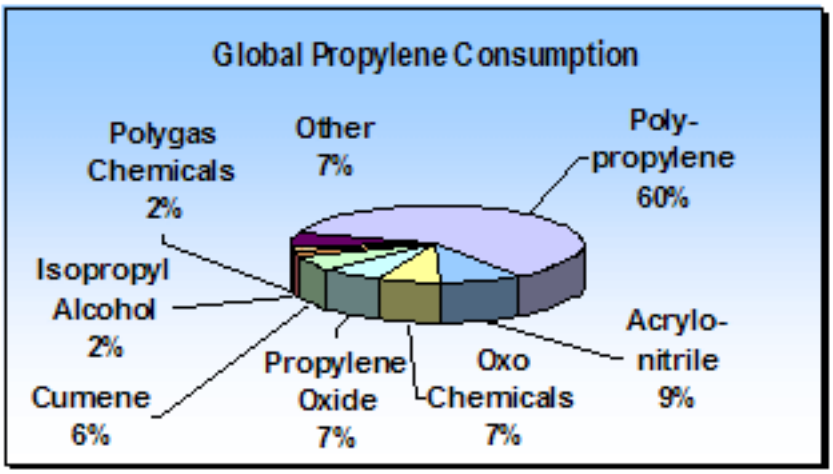

Figure 1: Global Propylene Consumption

Demand for propylene derivatives has begun to outpace production from traditional refineries, which are optimized for ethylene production [3] [4]. In 2010, the commodity price of propylene reached parity with that of ethylene [4] [5]. Due to expanded production of natural gas in the United States, propane has become an

increasingly viable feedstock for propylene production [4] [6]. Figure 2 shows the U.S. Department of Energy's projections for natural gas production over the next 30 years [7].

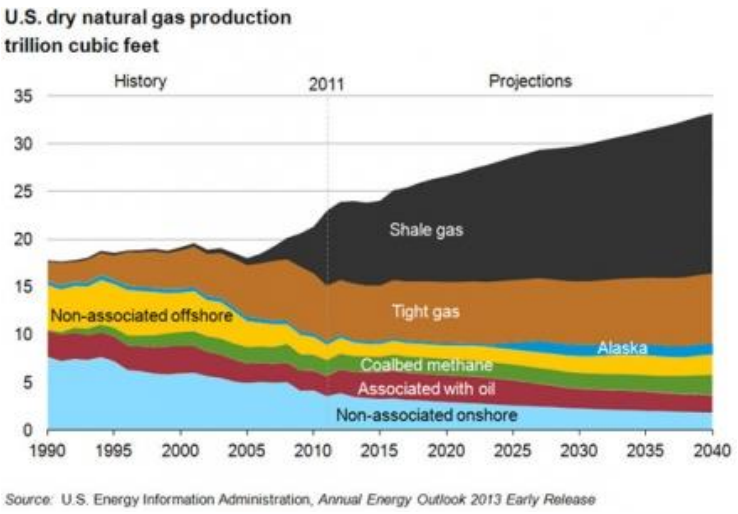

Figure 2: Estimated natural gas production in the United States

Propane can be converted to propylene via oxidative dehydrogenation (ODH). This reaction uses oxygen in the presence of a catalyst to selectively remove hydrogen from propane, forming the desired olefin. The right catalyst provides selective control of the reaction without fully oxidizing propane to carbon oxides. The stoichiometric equation for the ODH reaction is shown below in Equation 1. Losses due to partial and total combustion reactions are shown in Equations 2 and 3, respectively. Equation 4 shows the oxygen reduction reaction which takes place in specialized ODH reactors.

$$C_3H_8 + \frac{1}{2}O_2 \xrightarrow{Catalysts} C_3H_6 + H_2O \quad (1)$$

$$C_3H_8 + \frac{7}{2}O_2 \longrightarrow 3CO + 4H_2O \quad (2)$$

$$C_3H_8 + 5O_2 \longrightarrow 3CO_2 + 4H_2O \quad (3)$$

$$\frac{1}{2}O_2 + 2e^- \longrightarrow O^{2-} \quad (4)$$

Most catalysts for ODH are metal oxides which engage in a Mars-van Krevelen mechanism [8]. In this reaction scheme, the propane reacts with catalyst oxygen [8]. During the reaction, the catalyst is reduced when it loses an oxygen atom to form water [8]. The purpose of feeding gas phase oxygen is to re-oxidize the catalyst [8].

Current applications of the ODH reaction use a fixed bed reactor, where propane and oxygen are simultaneously fed over a catalyst bed, as in Figure 3 [8]. One problem with the fixed bed reactor design is that weakly adsorbed oxygen gas on the catalyst surface is thought to accelerate losses due to combustion. For this reason, higher oxygen partial pressures result in lower propylene selectivity [8] [9].

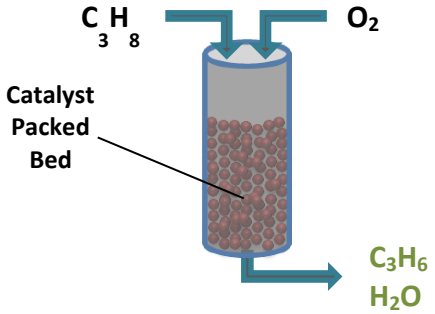

Figure 3: Packed bed reactor design

To improve the yield of propylene, membrane reactors have been proposed as a way to better control the contact of oxygen and propane on the catalyst active sites. These reactors typically have the propane and air feeds separated by a porous membrane. Oxygen diffuses across the membrane and is dispersed on the propane side of the reactor [8]. The membrane allows for locally reduced oxygen partial pressures, which increases the selectivity of alkene formation [8].

A novel type of membrane reactor which is investigated in this report uses a design similar to solid oxide fuel cells (SOFCs). In an SOFC, an ionically conductive electrolyte separates the fuel and air feed streams. At high enough temperatures, the cathode catalyst will reduce oxygen to oxide ions (See Equation 4). The oxide ions will conduct across the electrolyte to the anode, where it oxidizes the fuel. While this is happening, electrons are conducting on the wires surrounding the electrolyte, generating a current. A diagram of an SOFC is shown in Figure 4.

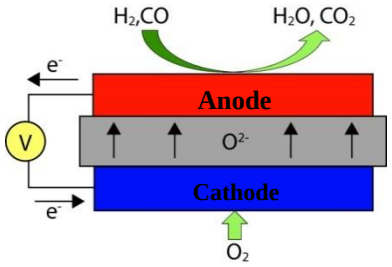

Figure 4: Solid Oxide Fuel Cell Diagram

For an ODH reactor, however, the operation is modified. Rather than withdrawing power, the reactor uses the electrical leads to apply a voltage to the system. By

controlling the voltage across the electrolyte, the oxide flux delivered to the anode is also controlled. In effect, the membrane acts as an oxide pump [10]. Because the propane is reacting with oxide ion species (O2-), and not gas phase oxygen, the selectivity of the reaction increases [11]. A diagram of the ODH reactor used in this report is shown in Figure 5.

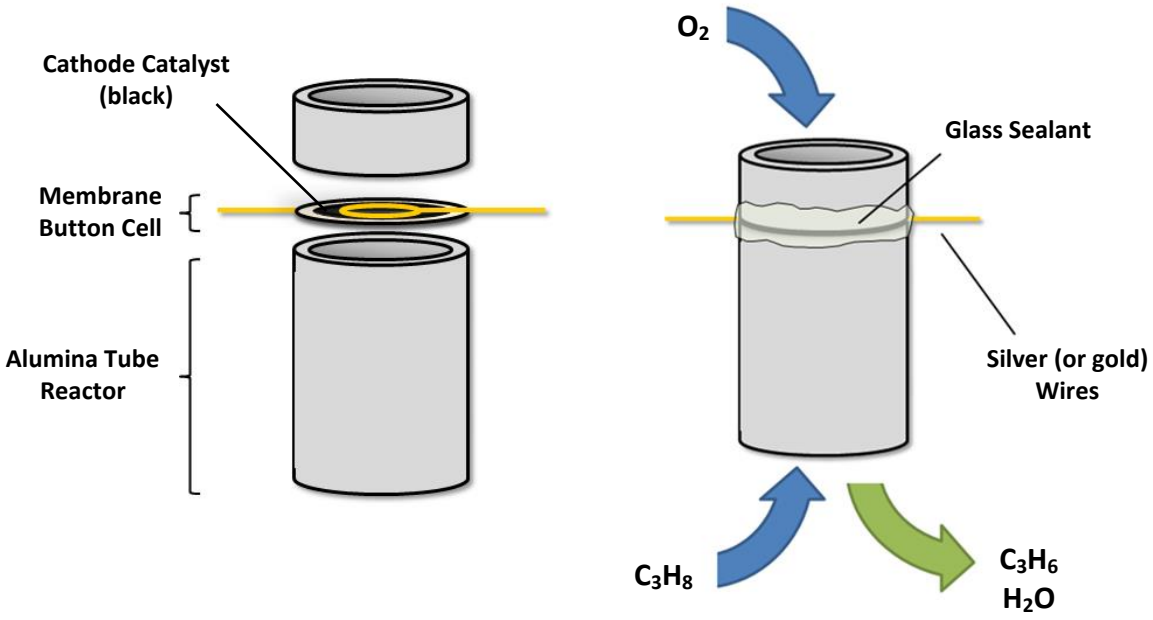

Figure 5: Electrochemical ODH Reactor

Despite the theoretical promise of an electrochemical ODH reactor, many challenges still exist. Because the cathode catalyst only activates at high temperatures (>700 °C), there are limited materials which can be used in the reactor setup [12] [13]. Our reactor (adapted from SOFC applications) uses a button cell supported on an alumina reactor tube. An above view of the button cell is shown in Figure 6. The button cell is a 1.5 cm diameter electrolyte disc with a cathode and an anode pasted to opposite sides.

The black material pasted in the center is the cathode catalyst, lanthanum strontium manganite (LSM). Extending from each side of the button cell are silver wires.

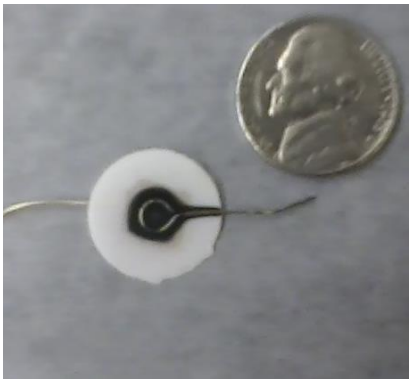

Figure 6: Above view of the button cell membrane (coin for scale)

For an electrochemical ODH reactor, it is important to be able to analyze the content of the product streams, and any air leaking into the system will cause inaccurate data. To ensure a hermetic seal, a glass-based adhesive is applied to the interface between the button cell and the alumina tube reactor (Figure 5).

In addition to sealing the reactor off from air leaks, it must also be able to produce stable electrochemical data. Unfortunately, unexplained jumps in the electronic current were recorded when the reactor temperature reached 800 °C (Figure 7). The hypothesis of this thesis was that the interference in the electric current was due to a reaction between the glass seal and the LSM in the cathode catalyst.

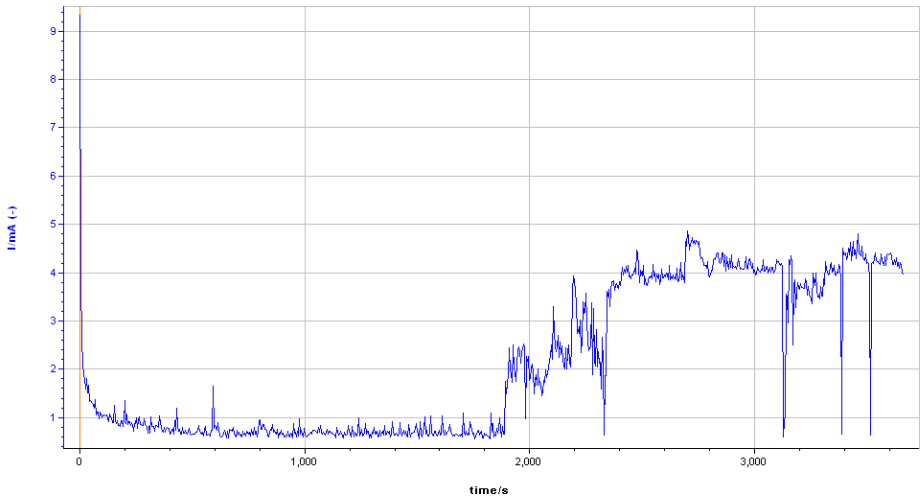

Figure 7: Current (mA) vs Time (s) at reactor temperature of 800 °C

Figure 8 shows the reactor tube column after curing the seal at 872 °C. The blackening of the glass contributes to the hypothesis that the glass seal is reacting with LSM. Glass based seals have been known to cause interference with catalysts in high temperature applications, and it is possible that boron species are forming separate phases with lanthanum and strontium [14].

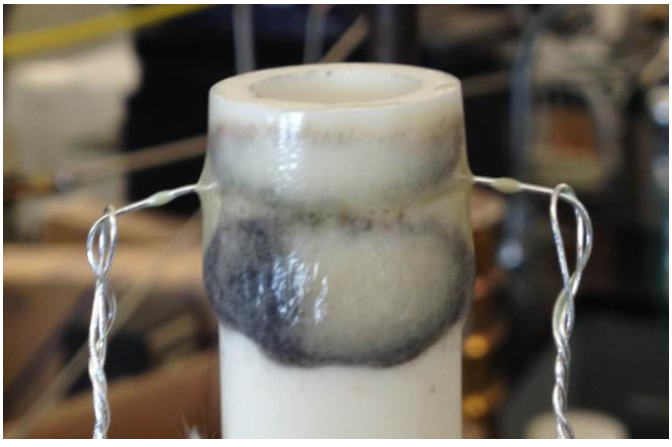

Figure 8: Side view of reactor with glass seal discoloration

Experimental

To characterize the interaction between the cathode and the seal, LSM and glass were mixed together and cured at 872 °C. Four powder samples were prepared containing different mass fractions of glass in LSM. Table 1 lists the samples prepared and their respective glass contents. The LSM-glass mixtures were prepared by dissolving them in 10 mL of deionized water. These aqueous mixtures were allowed to vaporize off at 90 °C before bringing the temperature up to 872 °C. After curing, the material becomes hardened, adhering to its calcination vessel. To remove LSM-glass and pure glass from the vessel, a hammer and chisel had to be used. Often times, this would destroy the vessel.

Table 1: Samples Prepared

Sample	Mass fraction of glass
LSM	0.00
LSM-glass (low loading)	0.25
LSM-glass (high loading)	0.50
Glass	1.00

The LSM in this project was synthesized by NexTech Materials, while the glass seal was produced by Aremco Products. Because the glass was made externally, we did not know its exact composition. Certainly, the main component is silicon dioxide, but

there are likely other elements present, such as boron, barium, calcium, etc. XPS was used to analyze changes in the surface composition of LSM.

Changes in the bulk structure of LSM were observed using X-ray diffraction (XRD). The recorded patterns were compared to a database. XRD patterns were used to determine which crystal phases were formed.

Results

Before analyzing the LSM-glass samples, it was important to define the composition of the glass seal. Table 2 a list of elements which can typically be found in glass sealants for SOFC reactors [15].

Table 2: Elements common to SOFC reactor glass seals [15]

Element
Aluminum
Barium
Boron
Calcium
Magnesium
Oxygen
Sodium

Figure 9 compares the XRD patterns between glass loadings of LSM samples. As the concentration of glass increases in the sample, the noise level in the data also increases. This is because glass is an amorphous solid, and does not have a well ordered crystal structure like LSM. The XRD pattern for the pure glass sample produced no signals, and was not included in this report. When LSM and glass were cured together, many new peaks were formed between $2\theta = 23$ and $2\theta = 31$. The formation of these new peaks suggests that a new structure was formed in the bulk phase.

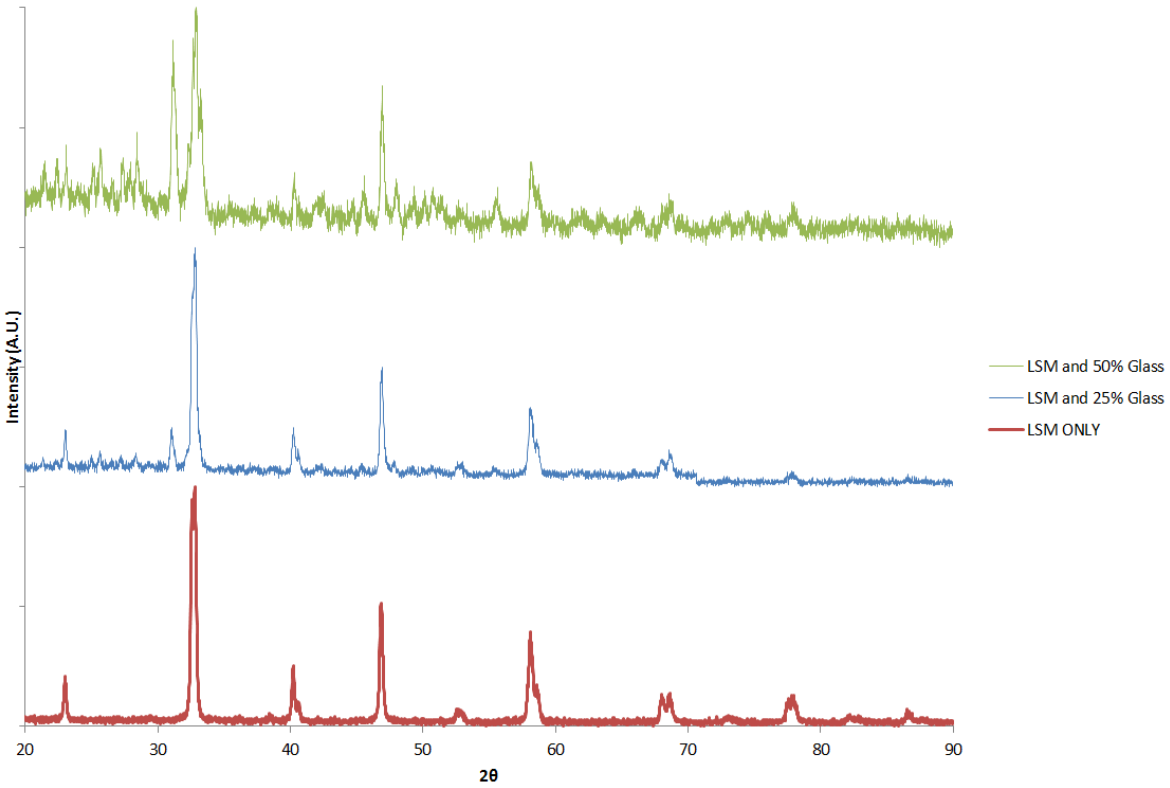

Figure 9: XRD patterns for different levels of glass loading in LSM

LSM-glass with a 25% loading was used to identify substances contributing to the newly formed peaks. Given the elements in the glass seal (listed in Table 1), XRD pattern databases could be searched for potential matches. Figure 10 shows a more detailed plot of the XRD pattern recorded for LSM0-glass 25%. The blue peaks are database listings for LSM, while the green peaks are for strontium lanthanum aluminate. It is important to note that the height of the peaks is not as important as their location on the horizontal axis. While there were no perfect matches for LSM-glass 25%, this XRD data suggests it may be forming a compound which belongs to the strontium aluminate family.

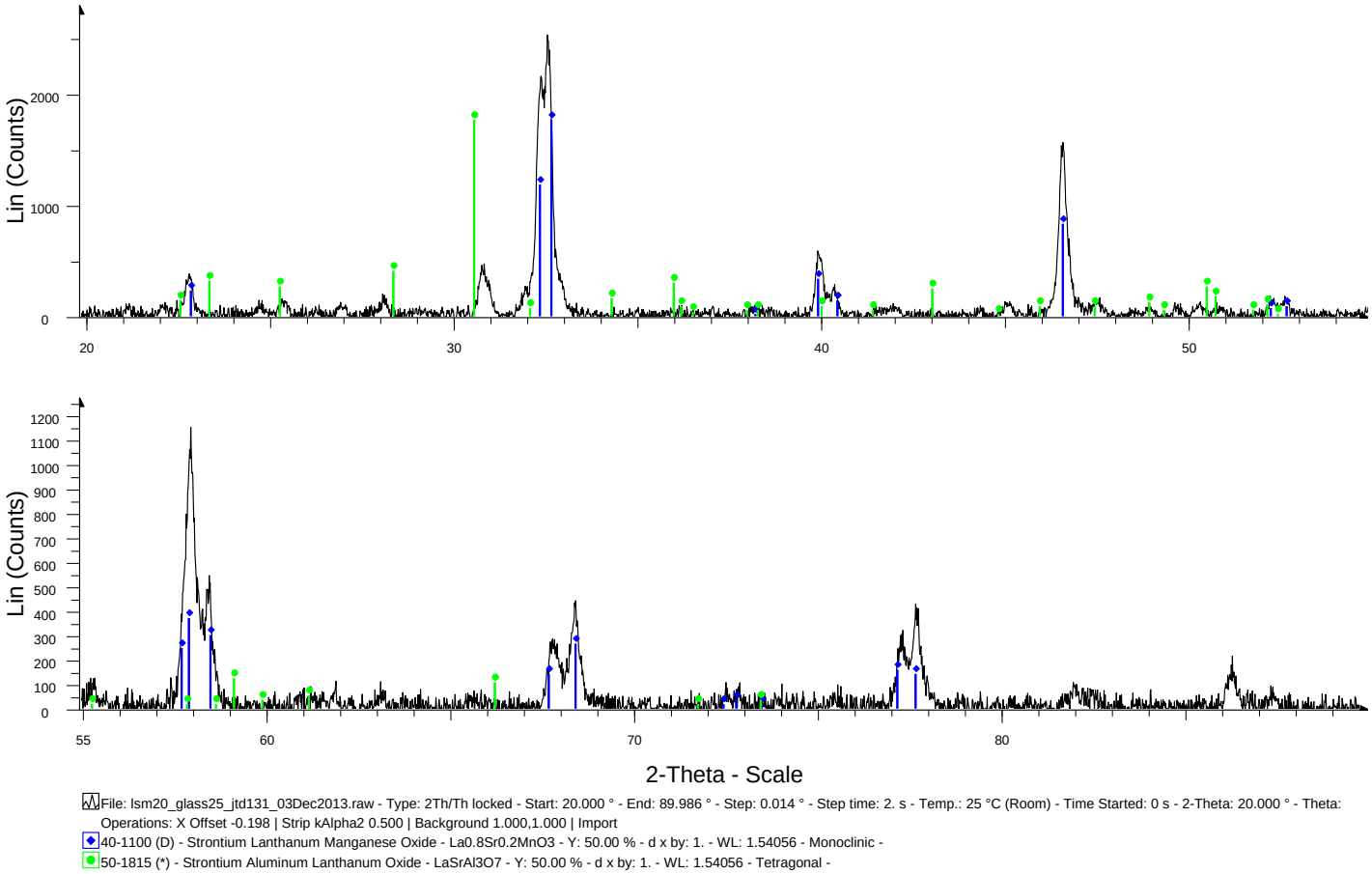

Figure 10: Strontium lanthanum aluminate and LSM XRD patterns

XPS data was collected in the La 3d and Sr 3d regions. The La 3d XPS spectra for each level of glass loading in LSM was compiled and organized into Appendix A1. The Sr 3d XPS spectra can be found in Appendix A2. Figure 11 shows the expected La 3d pattern for lanthanum perovskites found in literature [16] [17]. In XPS, 3d-electrons exhibit splitting, creating two distinct peaks called 3d (3/2) and 3d (5/2). The 3d (3/2) peak occurs at a higher binding energy level, but has an intensity equal to 2/3 the value of the 3d (3/2) peak. In Figure 11, there are two sets of La 3d electron peaks, giving a total of 4 peaks. The peak at 833.5 eV is due to La in a trivalent oxide, while the peak at 837 eV is due to hydroxyl formation on the surface.

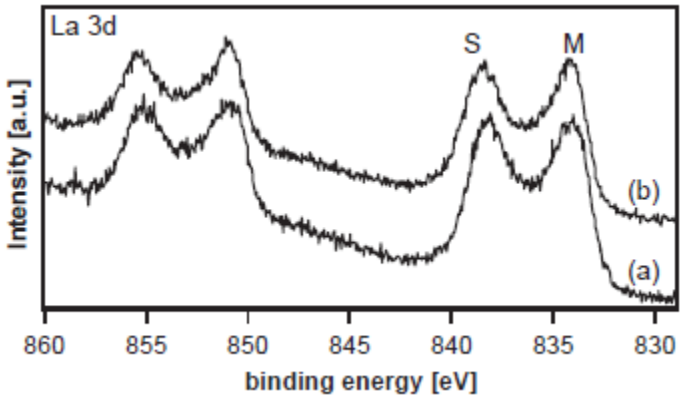

Figure 11: La 3d lines reported by Wu et al. [17]

Figure 12 shows the XPS spectra for Sr 3d which is typically reported for LSM [17]. Curve (a) is for LSM at room temperature while curve (b) is LSM after thermal treatment. The shoulder peak on the left is due to the formation of a strontium oxide phase.

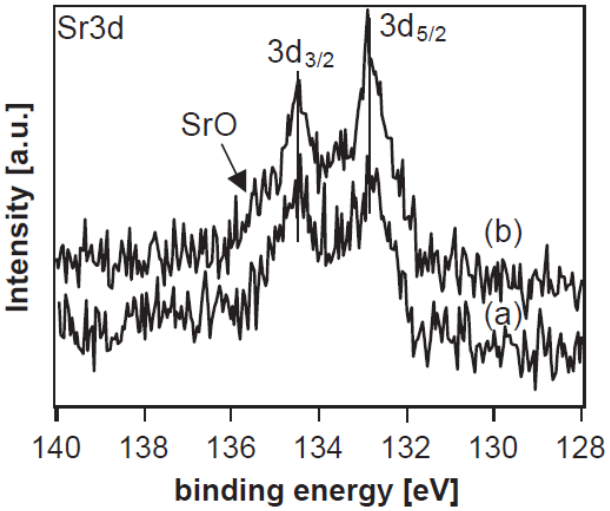

Figure 12: Sr 3d pattern for LSM (a) at room temperature and (b) after heat treatment [17]

Discussion

The formation of a peak at $2\theta = 31$ in Figure 9 and Figure 10 strongly suggests that the glass seal is reacting with LSM. While it was originally suspected that boron was causing the two materials to react, materials such as lanthanum borate and strontium borate could not be identified in Figure 10. There was also no evidence to suggest that the new phase belonged to lanthanum or strontium segregation to La_2O or SrO. The closest match was lanthanum strontium aluminate. This match is plausible, as aluminum was likely one of the elements in the glass seal. Unfortunately, the spectra for lanthanum strontium aluminate does not match perfectly with the peaks in Figure 10. Aluminates, however, tend to be semi amorphous and can have significant variance between diffraction patterns.

For XPS analysis, it was imperative to analyze the elements which are unique to LSM, lanthanum and strontium. While the O 1s pattern was also recorded, the results were not useful because oxygen exists in both LSM and the glass seal. Thus, any changes in the peak shape between glass loadings for O 1s could be attributed to there being a simple mixture of LSM oxygen and glass oxygen. Since lanthanum and strontium only exist in LSM, if their peaks change, it can be attributed to a surface interaction with the glass.

In Figures Figure 15, Figure 16, and Figure 17 in Appendix A1, the overall LSM 3d curve does not change drastically. The ratio of trivalent to hydroxyl lanthanum on the surface adjusts slightly, but overall each curve exhibits the same peaks.

For Sr 3d, however, there is a different story. In Figures Figure 18,Figure 19, Figure 20 (see Appendix A2), the peak at 131.5 eV confirms the divalent strontium which exists in LSM. At 133.6 eV, a second Sr 3d peak appears, and its relative area increases with increasing glass loading. Bukhtiyarova et al. reported a biding energy of 131.6 eV for strontium on the surface of strontium aluminates [18]. Figure 13 shows the reported Sr 3d curve in a strontium aluminate [18]. It should be noted that the x-axis in Figure 13 reports the binding energies in increasing order rather than decreasing order.

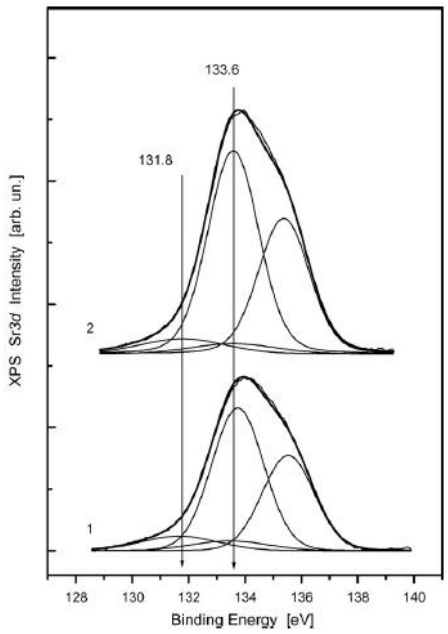

Figure 13: Sr 3d for a strontium aluminate [18]

While the results from XRD and XPS confirm that LSM and glass are able to react with each other at the curing temperature, the results do not confirm that this is the cause of interference in the electrochemical data. In the past, the button cells for the

reactor were constructed using silver wires. New button cells were constructed using gold wires instead. Figure 14 below shows the electrical current vs. time data recorded for a button cell with gold wires.

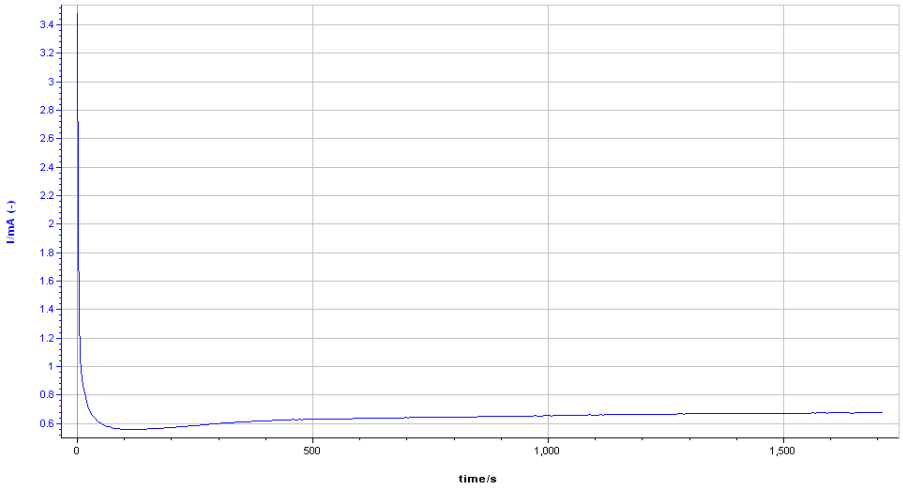

Figure 14: Current (mA) vs. Time (s) for a button cell using gold wires

Compared to Figure 7, Figure 14 exhibits much less noise. While LSM and glass may be reacting, it can be concluded that the wiring material is what caused the current to fluctuate. This is due to a number of reasons. For one, gold is inert. At 872 °C, silver could be reducing chemicals. Also, the melting point of silver is at 960 °C. If the reactor temperature fluctuates at high temperatures, silver could partially melt, causing the current data to jump. Gold, on the other hand, has a melting point of 1063 °C. Even at high reactor temperatures, it is unlikely to melt.

Conclusions

Electrochemical ODH is a promising process which can selectively produce propylene from propane. In order to carry out experiments in an ODH reactor, the button cell is sealed off from the atmosphere using a glass based sealant (Aremco glass seal-617). Instability in the electrical current data suggested that LSM was reacting with the seal. To investigate, LSM and Aremco glass seal-617 were cured together to see if they were reactive at high temperatures.

From XRD analysis, it was confirmed that a new phase formed. One material which seemed likely to form was lanthanum strontium aluminate. XPS data showed no significant changes in the surface composition of lanthanum, but strontium changed drastically. A new peak was observed which is also found to exist in strontium aluminates.

While LSM and glass are likely reacting, the conclusion cannot be drawn that it is causing instability in the electrical current across the button cell. By replacing the silver wires with gold ones, the button cell was able to maintain a stable current at high temperatures.

References

[1] S. Consulting, Chemical Economics Handbook, 2004.

[2] Dow Chemical Co., "Propylene," [Online]. Available: www.dow.com/productsafety/finder/pro.htm. [Accessed September 2013].

[3] A. Corma, F. Melo, L. Sauvanaud and F. Ortega, "Light cracked naptha processing: Controlling chemistry for maximum propylene production," *Catalysis Today,* Vols. 107-108, pp. 699-706, 2005.

[4] Chemsystems, "Evolving Propylene Sources — Solution to Supply Shortages?," 2012.

[5] P. Hodges, "Propylene Prices Reach Parity with Ethylene," ICIS, 12 July 2010. [Online]. [Accessed 10 September 2013].

[6] The Dow Chemical Company, "U.S. Gulf Coast Investments," [Online]. Available: http://www.dow.com/investors/presentations/pdfs/USGC_101211.pdf. [Accessed September 2013].

[7] U.S. Department of Energy, "Shale Gas R&D," [Online]. Available: http://energy.gov/fe/science-innovation/oil-gas/shale-gas-rd. [Accessed March 2014].

[8] C. A. Gärtner, A. C. van Veen and J. A. Lercher, "Oxidative Dehydrogenation of Ethane: Common Principles and Mechanistic Aspects," *ChemCatChem,* 2013.

[9] A. Kaddouri, "CH Bond Activation in the Presence of Absence of Oxygen or Nitrous Oxide," *React.Kinet.Catal.Lett.,* vol. 82, no. 2, pp. 401-409, 2004.

[10] K. Takehira, N. Sakai, J. Shimomura, H. Kajioka, S. Hamakawa, T. Shishido, T. Kawabata and K. Takaki, "Oxidation of C2-C4 alkanes over MoO3-V2O5 supported on a YSZ-aided membrane reactor," *Applied Catalysis A: General,* vol. 277, pp. 209-217, 2004.

[11] D. C. Creaser, B. Andersson, R. R. Hudgins and P. L. Silveston, "Kinetic Modelling of Oxygen Dependence in Oxidative Dehydrogenation of Propane," *The Canadian Journal of Chemical Engineering,* vol. 78, pp. 182-193, 2000.

[12] E. D. Wachsman and E. N. Armstrong, "Towards a Fundamental Understanding of the Oxygen Reduction Mechanism," *ECS Transactions,* vol. 35, no. 1, pp. 1955-1963, 2011.

[13] T. Yamaguchi, S. Shimizu, T. Suzuki, Y. Fujishiro and M. Awano, "Evaluation of Micro LSM-Supported GDC/ScSZ Bilayer Electrolyte with LSM-GDC Activation Layer for Intermediate Temperature-SOFCs," *Journal of the Electrochemical Society,* vol. 155, no. 4, pp. B423-B426, 2008.

[14] K. Chen, J. Hyodo, L. Zhao, N. Ai, T. Ishihara and S. P. Jian, "Effect of Volatile Boron Species on the MicroStructure and Composition of (La,Sr)MnO3 and (La,Sr)(Co,Fe)O3 Cathode Materials of Solid Oxide Fuel Cells," *Journal of The Electrochemical Society,* vol. 160, no. 9, pp. F1033-F1039, 2013.

[15] J. W. Fergus, "Sealants for Solid Oxide Fuel Cells," *Journal of Power Sources,* vol.

147, pp. 46-57, 2005.

[16] J. N. Kuhn and U. S. Ozkan, "Surface Properties of Sr and Co-doped LaFeO3," *Journal of Catalysis,* vol. 253, pp. 200-211, 2008.

[17] Q.-H. Wu, M. Liu and W. Jaegermann, "X-ray photoelectron spectroscopy of La0.5Sr0.5MnO3," *Materials Letters,* vol. 59, pp. 1480-1483, 2005.

[18] M. V. Bukhtiyarova, A. S. Ivanova, L. M. Plyasova, G. S. Litvak, V. A. Rogov, V. V. Kaichev, E. M. Slavinskaya, P. A. Kuznetsov and I. A. Polukhina, "Selective catalytic reduction of nitrogen oxide by ammonia on Mn(Fe)-substituted Sr(La) aluminates," *Applied Catalysis A,* vol. 357, pp. 193-205, 2009.

Appendix A1: La 3d XPS

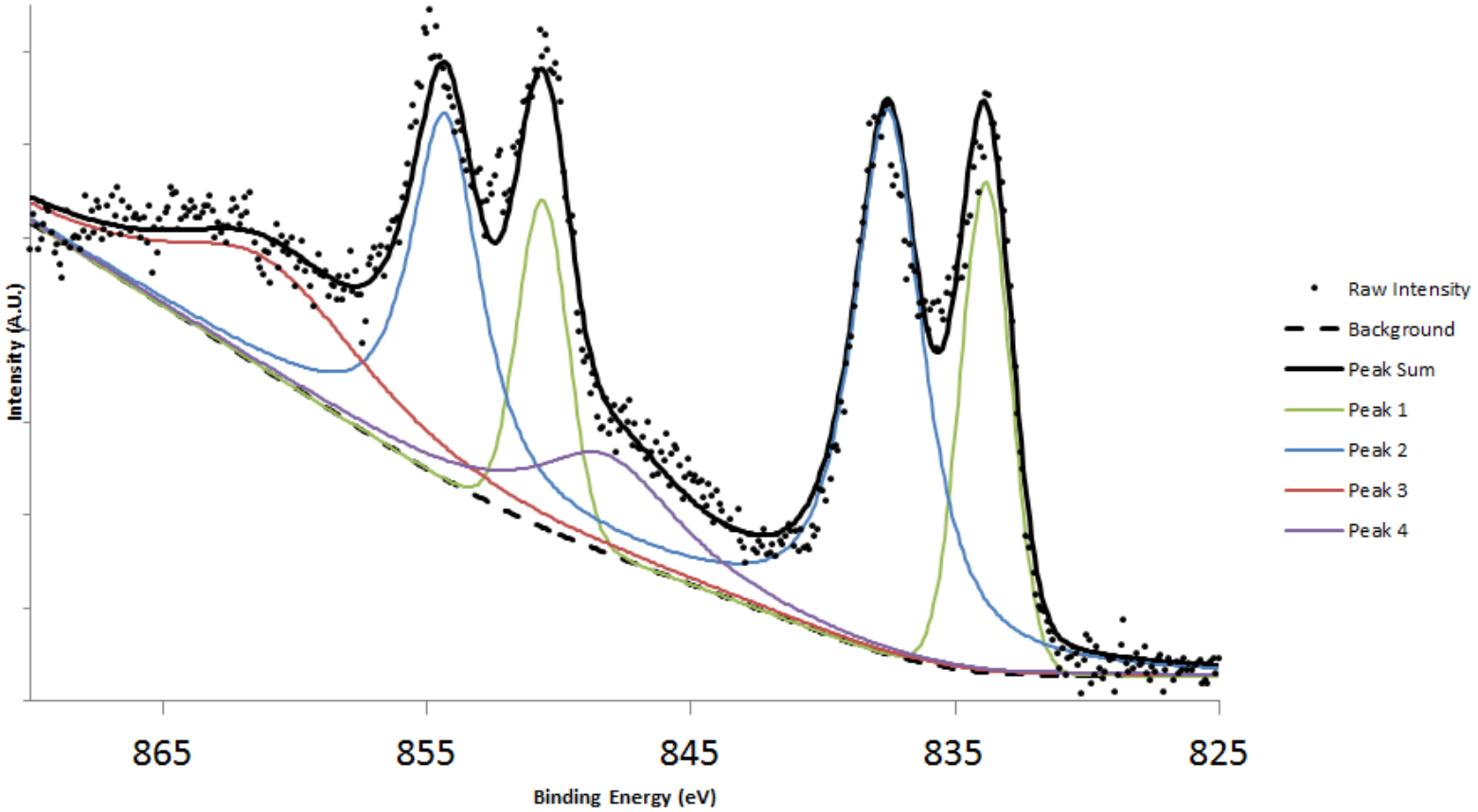

Figure 15: La 3d Pattern for LSM

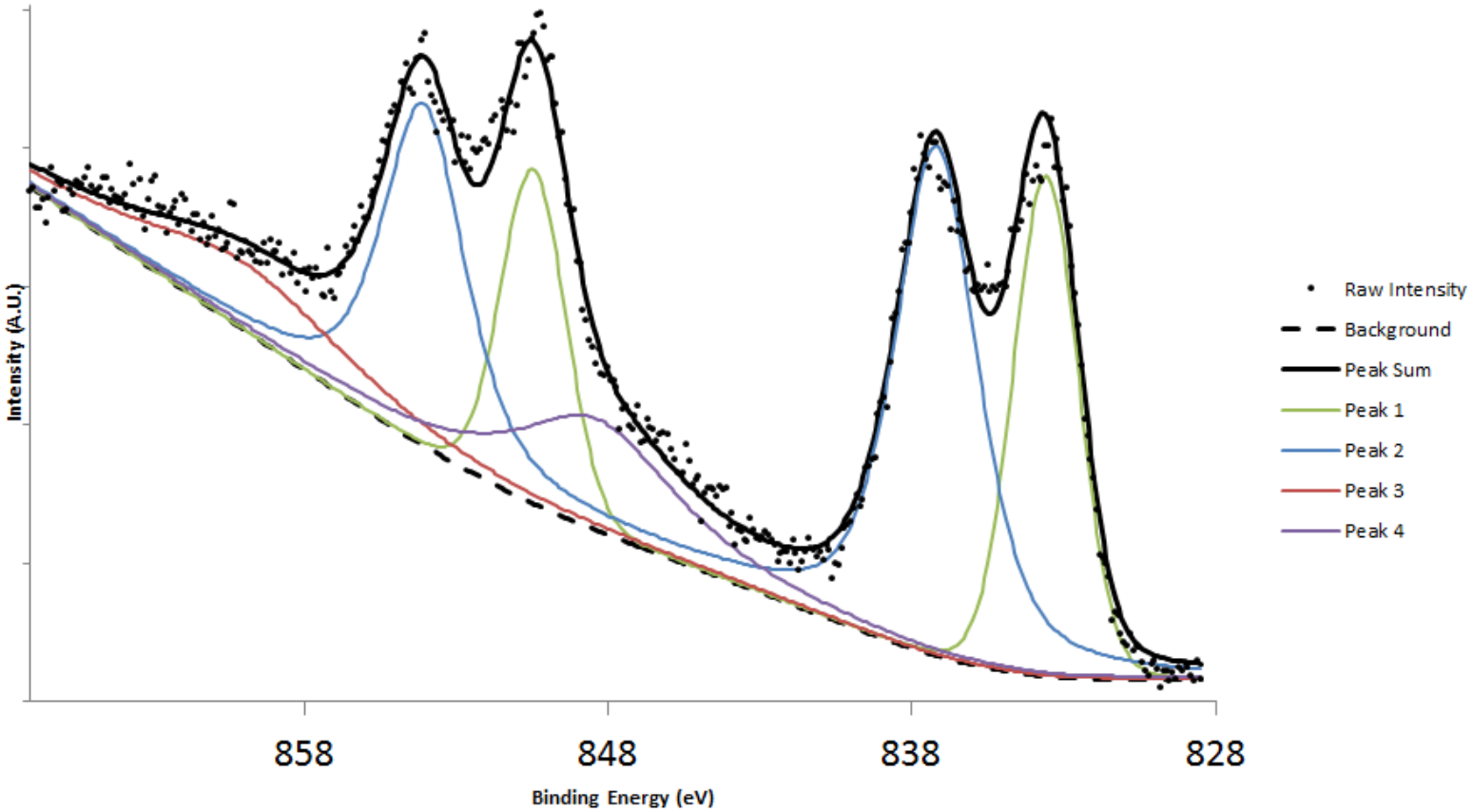

Figure 16: La 3d Pattern for LSM-Glass 25%

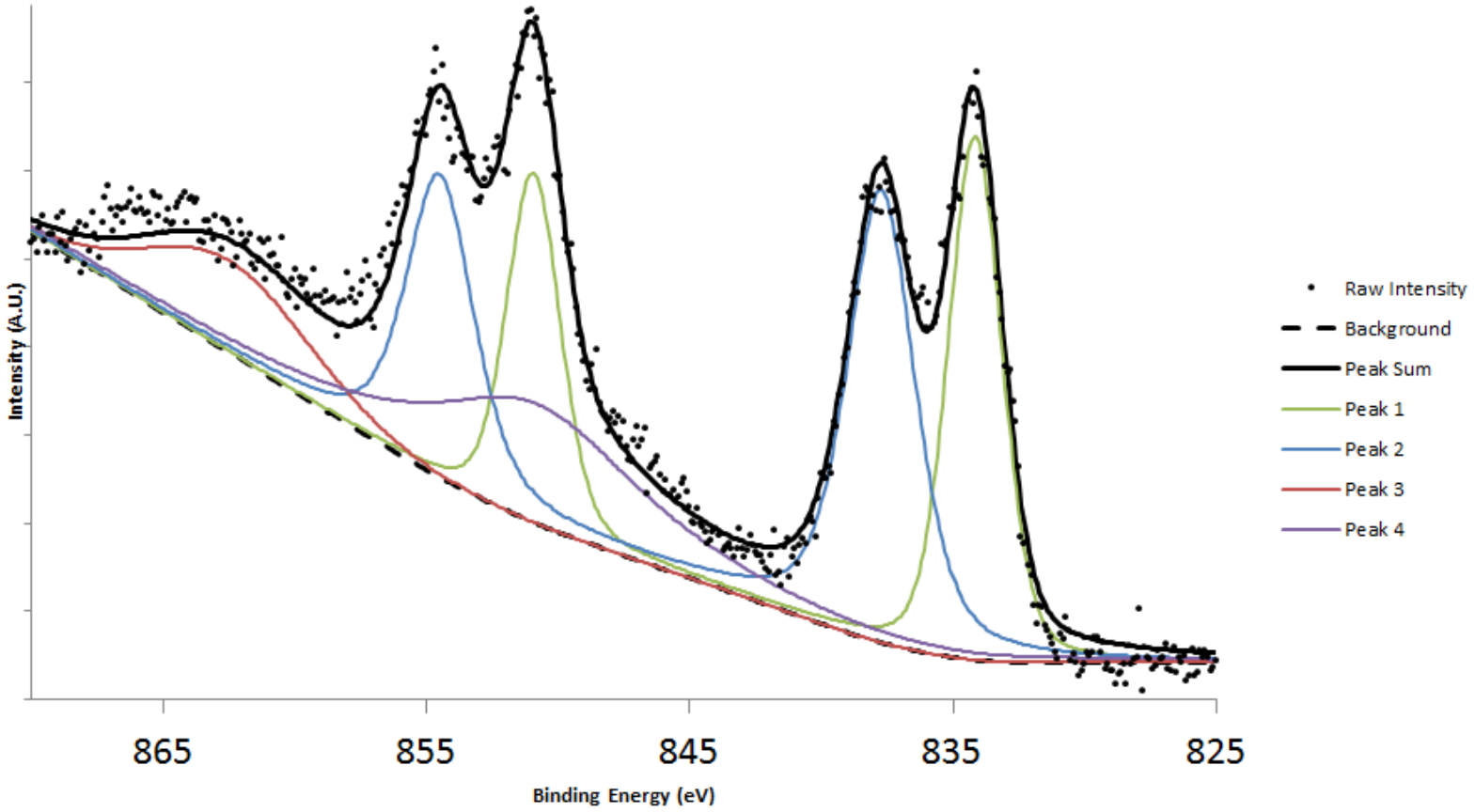

Figure 17: La 3d Pattern for LSM-Glass 50%

Appendix A2: Sr 3d XPS

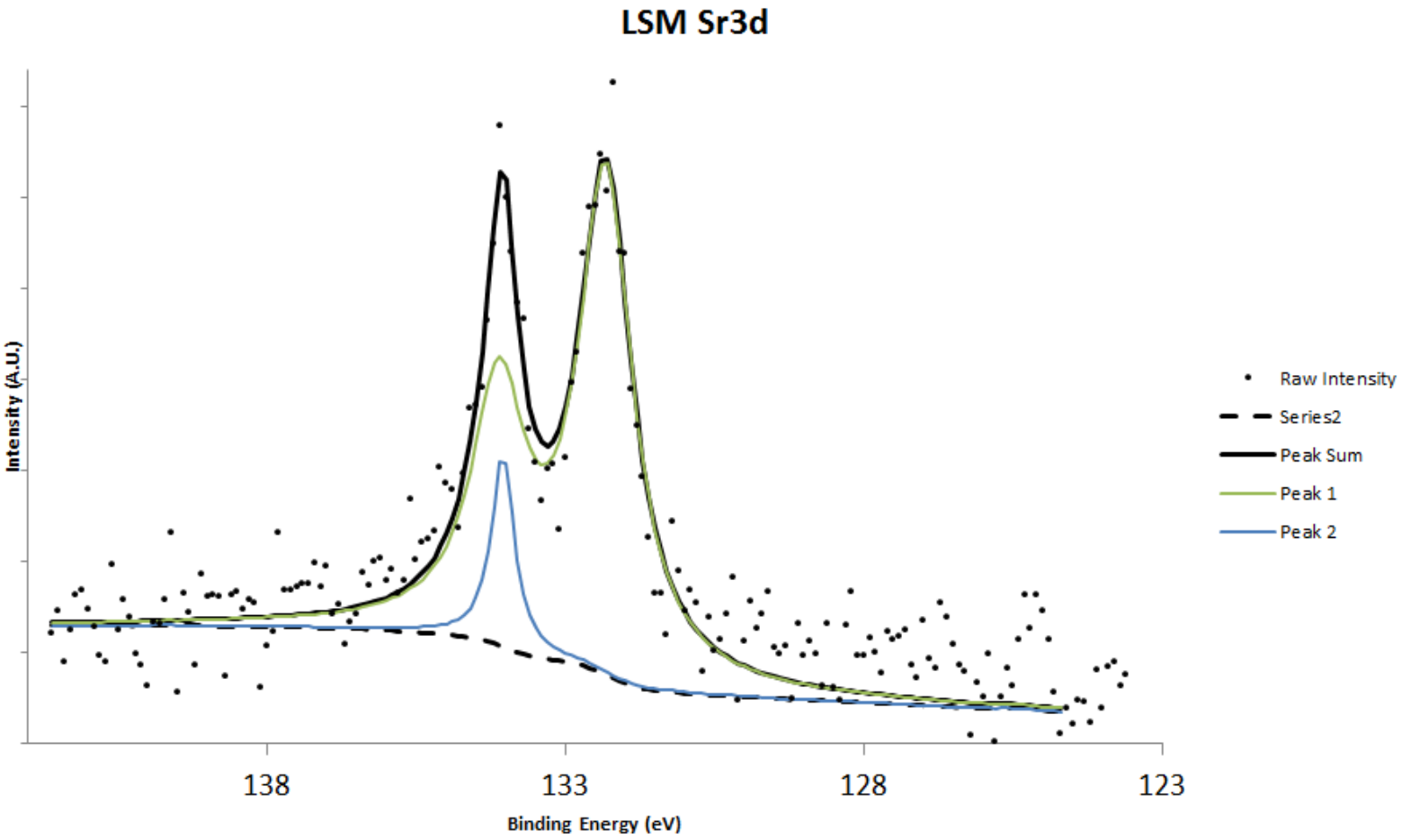

Figure 18: Sr 3d Pattern for LSM

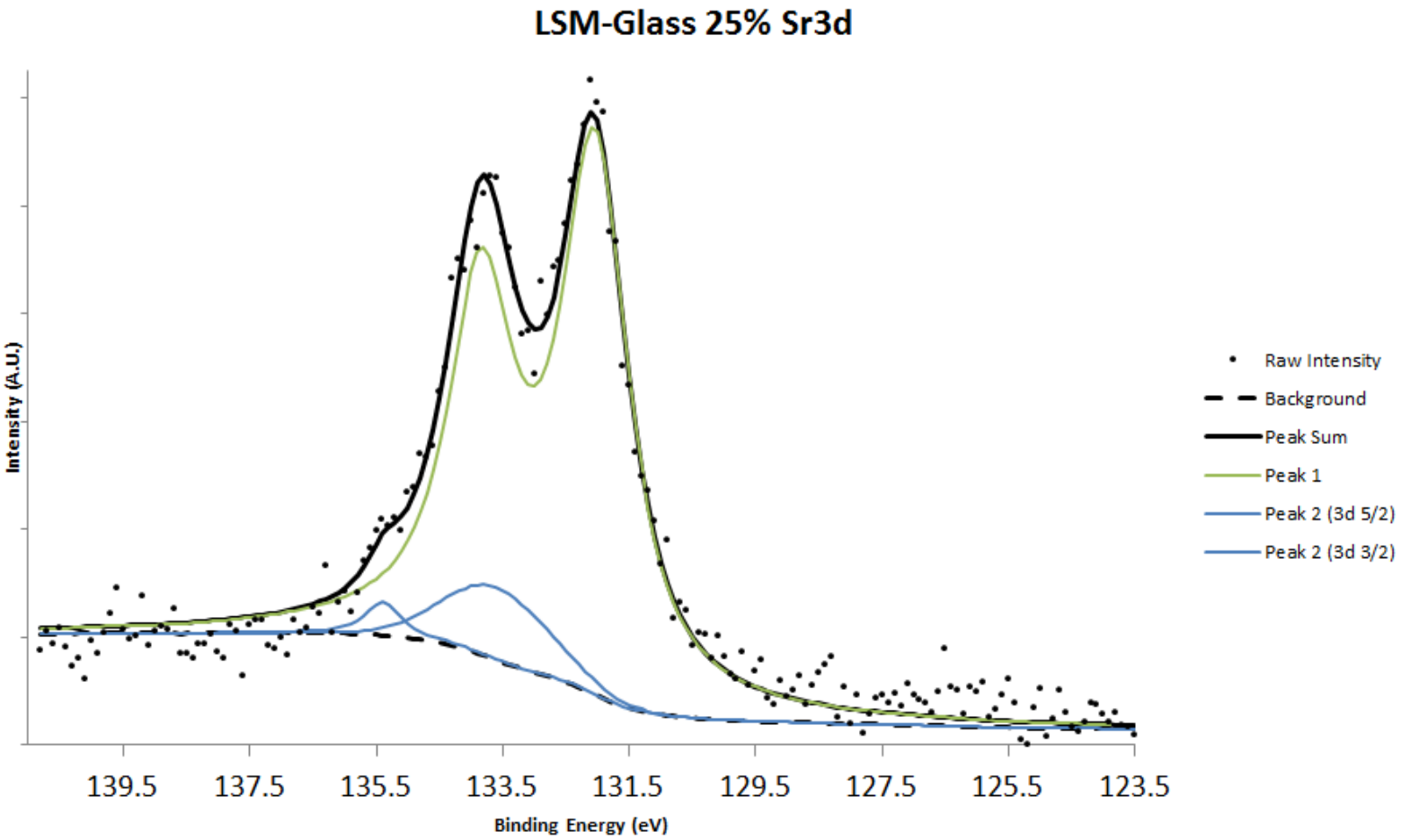

Figure 19: Sr 3d Pattern for LSM-Glass 25%

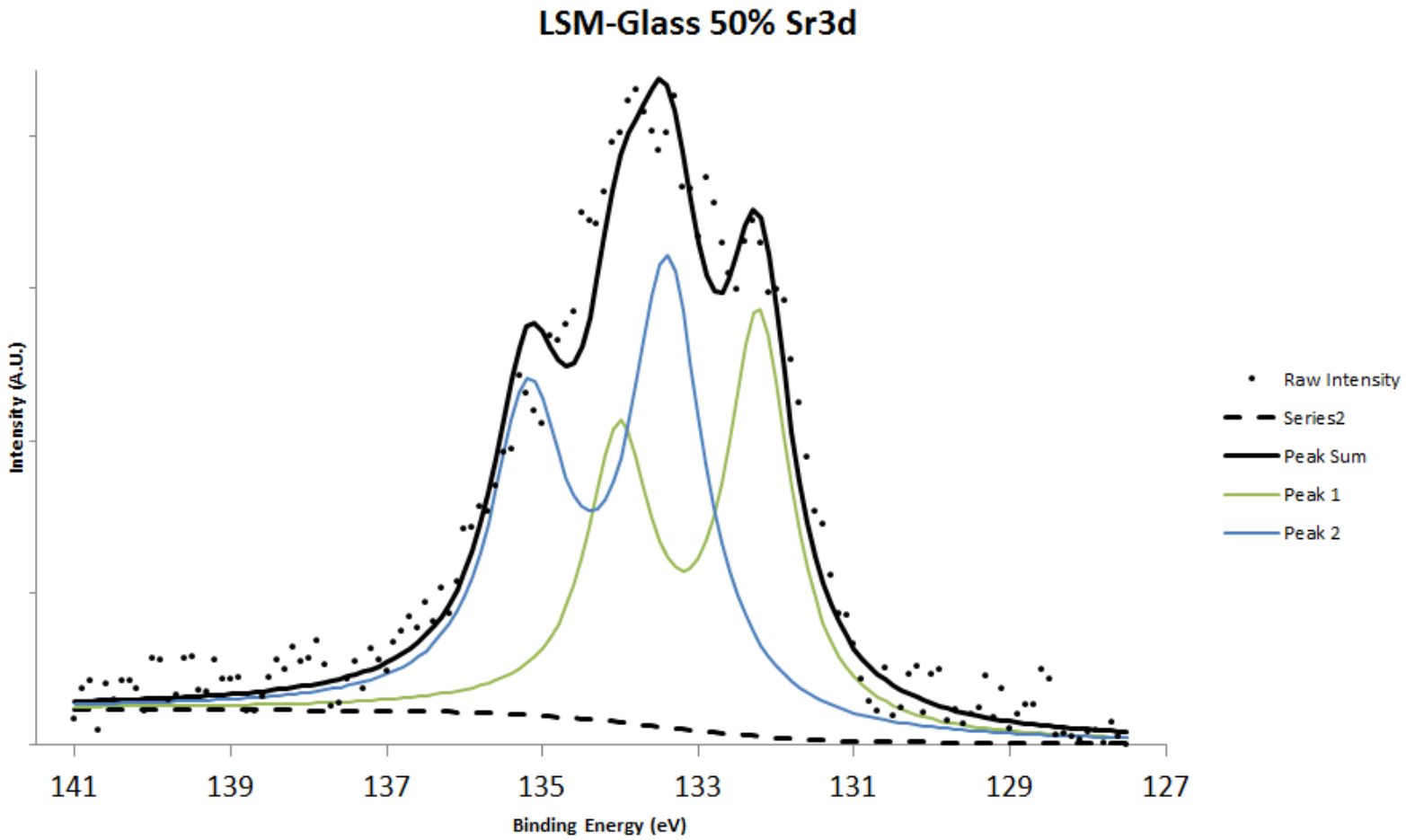

Figure 20: Sr 3d Pattern for LSM-Glass 50%